

# A spatial modeling framework for monitoring surveys with different sampling protocols with a case study for bird populations in mid-Scandinavia

Jorge Sicacha-Parada <sup>\*1</sup>, Diego Pavon-Jordan <sup>†2</sup>, Ingelin Steinsland <sup>‡1</sup>, Roel May <sup>§2</sup>, Bård Stokke <sup>¶2</sup>, and Ingar Jostein Øien <sup>||3</sup>

<sup>1</sup>Department of Mathematical Sciences. Norwegian University of Science and Technology (NTNU). Trondheim, Norway

<sup>2</sup>Department of Terrestrial Ecology, Norwegian Institute for Nature Research (NINA), P.O. Box 5685 Torgarden, N-7485. Trondheim, Norway

<sup>3</sup>Norwegian Ornithological Society-BirdLife Norway, Sandgata 30 B, NO-7012. Trondheim, Norway

## Abstract

Quantifying species abundance is the basis for spatial ecology and biodiversity conservation. Abundance data are mostly collected through professional surveys as part of monitoring programs, often at a national level. These surveys rarely follow exactly the same sampling protocol in different countries, which represents a challenge for producing biogeographical abundance maps based on the transboundary information available covering more than one country.

We here present a novel solution for this methodological challenge with a case study concerning bird abundance in mid-Scandinavia. We use data from national breeding bird monitoring programs in Norway and Sweden. Each census collects abundance data following two different sampling protocols that each contain two different sampling methods (i.e. these protocols generate data from four different sampling processes; see description of the protocols below). We propose a modeling framework that assumes a common Gaussian Random Field driving both the observed and true abundance with either a linear or a relaxed linear association between them. Thus, the models in this framework can integrate all sources of information involving count of organisms (four sources of bird count data in our case study) to produce one estimate for the expected abundance, its uncertainty and the covariate effects. Bayesian inference is performed using the Integrated Nested Laplace Approximation (INLA) and the Stochastic Partial Differential Equation (SPDE) approach for spatial modeling. We also present the results of a simulation study based on the empirical census data from mid-Scandinavia to assess the performance of the models under model misspecification. Finally, maps of the total expected abundance of the bird species present in our study region in mid-Scandinavia were produced.

We found that the framework allows for consistent integration of data from surveys with different sampling protocols. Further, the simulation study showed that models with a relaxed linear specification are less sensitive to misspecification, compared to the model that assumes linear association between counts. Relaxed linear specifications of bird abundance in mid-Scandinavia improved goodness-of-fit, but not the predictive power of the models.

---

\*jorge.sicacha@ntnu.no

†diego.pavon-jordan@nina.no

‡ingelin.steinsland@ntnu.no

§roel.may@nina.no

¶bard.stokke@nina.no

||ingar@birdlife.no

# 1 Introduction

Understanding why organisms are where they are and what drives changes in their abundances is one of the main pillars of spatial ecology (Brodie et al., 2020) and is critical to propose effective measures to preserve biodiversity. In this regard, species distribution models (SDMs) have typically been used to gain a better understanding of species-habitat relationships (Brodie et al., 2020) and to guide conservation practitioners, policy makers, and authorities (Araújo et al., 2019). Previous SDMs using abundance data have revealed higher predictive performance in comparison with those using occurrence data (Howard et al., 2014; Johnston et al., 2015). Yu et al. (2020) recently developed a method to include species abundance in Boosted Regression Trees (BRT) models (i.e. abundance-weighted approach) and concluded that their method was able to predict the distribution of (fish) species better than traditional (occurrence) BTR models, especially for rare and scarce species. Traditional BRT model, however, performed better for common species with higher prevalence (Yu et al., 2020). Abundance data have also proved important when disentangling the temporal, spatial and spatio-temporal effect of covariates (e.g. temperature) on bird abundances (Oedekoven et al., 2017). Yet, the majority of SDMs published to date used presence/absence (i.e. occurrence) data (Araújo et al., 2019; Yu et al., 2020), rather than abundance data (count of individuals), especially in large-scale studies. This limits our ability to robustly infer, for example, regions with high density of individuals (Johnston et al., 2015). Identifying such areas is of paramount importance, for example, to include them in the network of protected areas (e.g. Natura 2000 under the European Union’s Birds Directive, 2009/147/EC 2009, Brodie et al. (2020)), or to detect areas where human-wildlife conflicts may arise (e.g. Stroud et al. (2017)), informing the corresponding authorities that infrastructure developments such as siting of power lines and wind farms must be planned carefully (e.g. May et al. (2020)).

The scarcity of studies applying large-scale abundance SDMs is likely related to (i) the generally lower availability of abundance data compared to occurrence data as the former are more costly to gather than the latter and thus are restricted to small spatial scales or otherwise to certain groups of species through national monitoring programs, and (ii) statistical and computational challenges of modelling abundance data (e.g. overdispersion, zero-inflation, computational resources demand).

National breeding bird monitoring programs provide the largest datasets on species abundance in time and space. Data from such surveys have mainly been used to assess changes in biodiversity at the (sub)national level (Kålås, 2010; Bevanger et al., 2014; Kéry and Royle, 2009; Soykan et al., 2016) or to model temporal trends in species abundances (Lehikoinen et al., 2014, 2019). Previous multi-country studies have analyzed these data independently for each country to later draw common conclusions from the country-specific estimates (Lehikoinen et al., 2019). In Kéry and Royle (2009) and Soykan et al. (2016) hierarchical models with random effects associated to temporal autocorrelation, observer effect, and detectability are recurrent choices. Fusion between monitoring surveys and capture-recapture data has also been proposed as a way to improve inferences (Ahrestani et al., 2017).

This study was motivated by the need to estimate the abundance of birds in mid-Scandinavia, based on high quality but localized data on bird abundances gathered as part of the common breeding bird monitoring programs in Norway (TOV-E) and Sweden (BBS). However, the TOV-E and the BBS differ in their protocols. Although both countries collect observations in point counts and transect surveys, in Norway line transects are complementary (only a subset of species are recorded) to the main point counts (all species recorded) whereas line transects and point counts in Sweden are regarded as two different independent censuses (e.g. all species are counted in both census methods). These differences present the challenge of integrating the four sources of spatial information (points and transects in both Norway and Sweden) with different sampling protocols into one estimate for the spatial distribution of bird abundance for the entire region of interest (Brodie et al., 2020; Gruss and Thorson, 2019).

Here we present a generic modelling framework that uses a combined dataset of abundance data from various monitoring schemes with different sampling protocols to produce one single estimate of local species abundance and its uncertainty. In addition, it also gives interpretable estimates of the ecological parameters driving species abundances. Thus, unlike previous studies using multi-country abundance data, we aim to

analyze these data in a unique, single framework to produce models that describe and predict the spatial distribution of abundances rather than using the temporal autocorrelation of these data to forecast counts in future scenarios.

Spatial modeling of multiple data sources has been approached for example in the context of coregionalization models (Banerjee et al., 2015; Blangiardo and Cameletti, 2015; Krainski, 2019). These are multivariate models for measurements that vary jointly over a region and have been defined through a hierarchical structure and fitted using Markov Chain Monte Carlo (MCMC) techniques (Banerjee et al., 2015). For the family of Spatial Latent Gaussian Models (Rue and Held, 2005), the INLA-SPDE approach (Rue et al., 2009; Lindgren et al., 2011) and its easy implementation in the INLA library of R have emerged as a faster alternative to jointly model multiple sources of information. Such method has been applied to multivariate models related with, for example, air pollution data (Cameletti et al., 2019) and hydrology (Roksvåg et al., 2020). The proposed framework lies within the class of Spatial Latent Gaussian Models and, in principle, relies on two main assumptions. First, the existence of a common Gaussian Random Field that drives the observed counts of each data source, and second, a linear relation between the observed counts and the true abundances determined by each observation process. Given that the latter assumption makes our models less flexible and may not depict the true relationship, we in addition propose models that allow us to account for deviations from linear association between the observed counts for different protocols. These models are suitable for being fitted using the INLA-SPDE approach, which approximates the posterior densities of parameters and hyperparameters. Furthermore, this method represents Gaussian Random Fields as discrete indexed Gaussian Markov Random Fields (GMRF) to produce faster inferences. Such a methodology on modeling spatial abundance using data from multi-country biodiversity monitoring programs with different sampling protocols has, to the best of our knowledge, not been published before. This study, therefore, opens possibilities for international assessments of species distributions using abundance data from diverse national monitoring programs, which is of paramount importance for understanding global change impacts on biodiversity. We validate this framework through the aforementioned case study of bird species abundance in mid-Scandinavia and a simulation study that explores the effects of misspecification on the proposed models.

This paper is organized as follows: In Section 2, we describe the data from the Norwegian and Swedish monitoring programs in detail. Moreover, we explain how we preprocessed these census data, present an exploratory analysis and introduce the set of candidate explanatory variables for our models. In Section 3, models as well as inference methodology and measures for evaluating and comparing them are presented. In Section 4, we carry out a simulation study showing how differently the proposed models perform in scenarios with different assumptions about the relation between the observed and the true abundances. In Section 5, results of both the simulation study and the mid-Scandinavian bird abundance case study are presented. The paper finishes in Section 6 with the discussion of the results and concluding remarks.

## 2 Bird monitoring surveys data

### 2.1 TOV-E and BBS data

The Norwegian common bird monitoring scheme (TOV-E), coordinated by the Norwegian Institute for Nature Research (NINA) and the Norwegian Ornithological Society (NOF) since 2006, was established to monitor population variation for common breeding terrestrial birds on a national scale in a representative way. Surveys (i.e. count of pairs of birds of all observed species) are carried out by experienced ornithologists that follow a standardized protocol Kålås and Husby (2002). Each census route ( $n = 492$ ) contains between 12 and 20 (average = 18.8) point counts 300 m apart describing a square (see Fig. 1) with side = 1.5 km (deviation of this shape are allowed and recorded when the geographic/topographic conditions do not allow the observer to walk, e.g. sea/lakes, glaciers, rough mountainous terrain). At each census route, all observers must record all the species ( $n = 229$ ) heard or seen at each of the point counts during 5 minutes. A random selection of 370 census routes (out of a total of 492 routes across Norway) are visited once a year during the period 20th May to 10th June. There are some species that are less abundant or whose detection is difficult. Hence, observers are asked to record these species ( $n = 121$ ) also during the line transect in-between the point counts (see Figure 1 - figure with the configuration of a census site with the twenty points). TOV-E

is designed to cover all relevant habitats throughout the altitudinal and latitudinal gradient in Norway and reports ‘pairs of individuals’ as sampling unit.

The Swedish breeding bird survey (hereafter BBS) is coordinated by Lund University since 1996 and consists of 716 fixed sites across Sweden within a 25-km grid (one route per grid cell, see Lindstrom et al. (2013)). These sites are surveyed once a year between mid-May and mid-June (the breeding period for most bird species in Sweden) though not all sites are surveyed every year (mean = 353 sites per year). The 25-km grid makes sure that the habitats of Sweden are monitored in proportion to their abundance in the country as well as the entire altitudinal and latitudinal gradient where birds are present. At each site, the observer walks an 8-km transect describing a  $2 \times 2$  km square and records all bird species heard and/or seen within 8 h. In addition, the observer has eight 5-min point counts where all birds seen or heard must also be recorded. The point counts take place at each of the corners of the square and in the centroid of the square. Of the circa 250 species breeding in Sweden, 244 are reported in BBS, thus ensuring a good coverage of the breeding birds (Lindstrom et al., 2013). The BBS reports ‘individuals’ as sampling unit, which differs from TOV-E’s reporting unit (pairs of individuals; see above).

For our case study, we only selected census sites that lie within a polygon defined to produce an approximation of a Gaussian Random Field when we want to make inference about a point pattern in Trøndelag (see red polygon in Fig. 1, (Lindgren et al., 2011; Simpson et al., 2016)). This polygon covers a total area of  $173.634 \text{ km}^2$  and contains 113 census sites in Norway and 70 in Sweden.

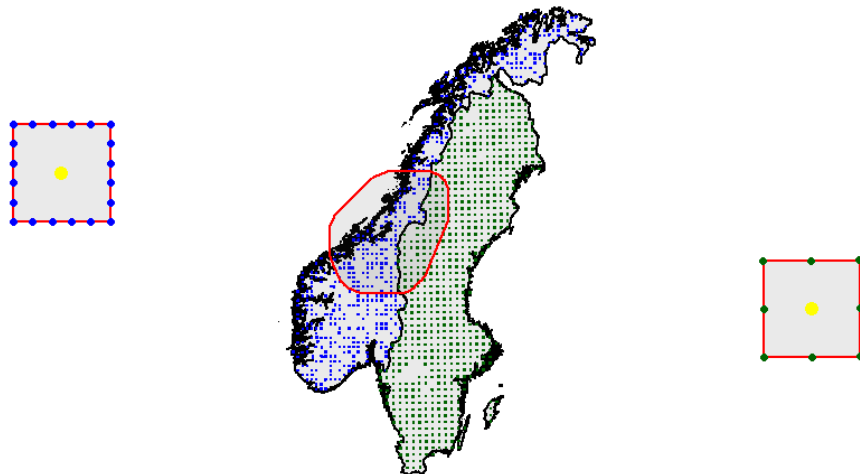


Figure 1: Spatial location of census sites and sampling points and line transects according to each sampling protocol. Left: Graphical display of sampling protocol of TOV-E census. Blue points: 20 locations for point counts (the number of points vary between 12 and 20 in the different sites). Red lines: Line transects. Yellow point: Centroid associated to each census site (see Section 2.2). Center: Spatial distribution of census sites across Norway (blue sites) and Sweden (green sites). The red polygon represents the study area described in Section 2.1. Right: Graphical display of sampling protocol of BBS census. Green points: 8 locations for point counts. Red lines: Line transects. Yellow point: Centroid associated to each census site (see Section 2.2)

## 2.2 Exploratory Analysis

Our main goal was to detect hotspots of overall bird abundance, i.e. we are not interested in the distribution of particular species. Hence, we averaged the total count of all bird species found at each site across all years (2006 – 2019). That is, we first added up the counts of all bird species recorded in the points or lines of a given census site and assigned the total count to site’s centroid (see Figure 1). Next, for each site, we averaged all counts observed from 2006 to 2019 ( $n=15$  years). Since we include data from both Norway and Sweden, we explore how the relation of point and line counts differ between surveys from both countries. In

Figure 2, we display a scatterplot with the points and line counts at each of the TOV-E (n=113) and BBS (n=70) sites.

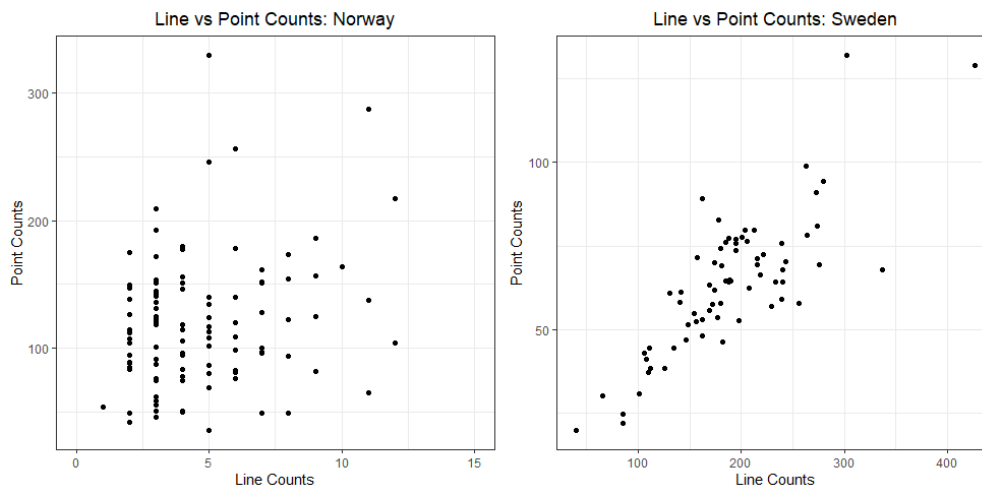


Figure 2: Scatterplots of line vs point counts in Norway (pairs, left) and Sweden (individuals, right)

These scatterplots show a linear relation between point and line counts in Sweden, whereas in Norway there is no clear linear association between the counts in points and lines. This is somehow expected due to the census design in Norway, where the line counts are meant to record a reduced subset of species compared to the point counts.

### 2.3 Explanatory variables

Our case study aims to produce abundance maps of bird species based on multiple sources of information. Moreover, we want to produce interpretable estimates of ecological factors associated with higher abundances. The candidate ecological factors for explaining abundances in the entire region are: (i) temperature (average daily temperature from April to July over 2006-2019, downloaded from seNorge.no), (ii) precipitation (average daily temperature from April to July over 2006-2019, downloaded from seNorge.no), (iii) elevation (Digital Elevation Model at a 10m resolution, DEM10, downloaded from <https://kartkatalog.geonorge.no/>), and (iv) the land cover surrounding each location expressed as the percentage of each of the following six land covers (urban, mountains, rocky area, water body, forest, and open area) in a square neighborhood of  $2km \times 2km$ . Land cover information was depicted from the N50 layer (downloaded from <https://kartkatalog.geonorge.no/>). All rasters files have resolution of  $1km \times 1km$  (the elevation data from DEM10 was aggregated to this resolution prior analysis) and are shown in the Supplementary Information.

As a first stage of model selection, we computed the correlation coefficient between all the candidate covariates on a fine grid of about 600.000 points. Only one variable in those pairs with  $|\rho| > 0.7$  was left as a candidate. Those pairs with high correlation were: 1) Elevation and temperature ( $\rho = -0.81$ ). Temperature was discarded; 2) % of open area and % of forest ( $\rho = -0.83$ ). % of open area was discarded.

## 3 Modeling and inference approach

The specification of our models relies on the assumption that our four sources of observations are obtained from a common underlying ecological process. This assumption arguably makes sense if we consider the fact

that national borders are not a key factor for natural changes in biodiversity. Hence, we can assume that a common non-zero mean Gaussian Random Field (GRF) is involved in the generation of the number of individuals at each census site. However, the two different sampling protocols (points and lines), which also differ between the two countries (complementary surveys in Norway and independent surveys in Sweden), result in four groups of counts observed. Moreover, TOV-E counts (Norway) are reported as ‘number of pairs’ of each species whereas BBS counts (Sweden) are reported as ‘number of individuals’ of each species. Therefore, direct inference and comparisons between these four response variables should be made with caution.

The true bird counts random variable,  $Y_{true}(\mathbf{s})$  with  $\mathbf{s} \in D \subset \mathbb{R}^2$  is assumed to follow a Poisson distribution with expected value  $\lambda_{true}(\mathbf{s})$ , expressed as

$$\log(\lambda_{true}(\mathbf{s})) = X^T(\mathbf{s})\beta + \omega_1(\mathbf{s}) \quad (1)$$

with  $X^T(\mathbf{s})$  a set of spatial covariates and  $\omega_1(\mathbf{s})$  a zero-mean GRF that aims at accounting for residual spatial autocorrelation. We assume a Matérn covariance function for  $\omega_1(\mathbf{s})$

$$\frac{\sigma^2}{\Gamma(\nu)2^{\nu-1}} (\kappa\|s_i - s_j\|)^\nu K_\nu(\kappa\|s_i - s_j\|) \quad (2)$$

with  $\|s_i - s_j\|$  the Euclidean distance between two locations  $s_i, s_j \in D$ .  $\sigma^2$  stands for the marginal variance, and  $K_\nu$  represents the modified Bessel function of the second kind and order  $\nu > 0$ .  $\nu$  is the parameter that determines the degree of smoothness of the process, while  $\kappa > 0$  is a scaling parameter. For  $\omega_1(\mathbf{s})$ , let  $\kappa = \kappa_1, \nu = \nu_1$  and  $\sigma^2 = \sigma_1^2$ .

We assume that the observed counts for each sampling protocol are realization of four random variables conditionally independent given  $\omega_1(\mathbf{s})$ . That is, we assume the four groups of observed counts are realizations of the Poisson random variables:

$$\begin{aligned} Y_1(\mathbf{s}) &\sim \text{Poisson}(\lambda_1(\mathbf{s})) && \text{(Point counts in Norway)} \\ Y_2(\mathbf{s}) &\sim \text{Poisson}(\lambda_2(\mathbf{s})) && \text{(Line counts in Norway)} \\ Y_3(\mathbf{s}) &\sim \text{Poisson}(\lambda_3(\mathbf{s})) && \text{(Point counts in Sweden)} \\ Y_4(\mathbf{s}) &\sim \text{Poisson}(\lambda_4(\mathbf{s})) && \text{(Line counts in Sweden)} \end{aligned}$$

where  $\lambda_j(\mathbf{s})$ ,  $j = \{1, 2, 3, 4\}$  are the expected values of the random variables  $Y_j(\mathbf{s})$ . Additionally, we assume  $\lambda_1(\mathbf{s}) + \lambda_2(\mathbf{s}) \approx \lambda_{NO}(\mathbf{s})$  as a proxy for total abundance since the line transects are complementary to the point counts in Norway. This assumption does not hold for Sweden since, as mentioned in Section 1, line transects and point counts are regarded as two different independent censuses. In case we wanted to suggest a proxy for the total abundance in Sweden using  $\lambda_3(\mathbf{s})$  and  $\lambda_4(\mathbf{s})$ , we would need to account for a potential overlap (double counting) between the counts observed in points and line transects. Our final assumption is that there are no differences in observer skills between countries since the census are performed by experienced ornithologists .

## 3.1 Models

### 3.1.1 Model 1

Based on our exploratory analysis and the four sampling processes present in our dataset, in model 1 we assumed a linear relation between the expected values of the four random variables and  $\lambda_{true}(\mathbf{s})$ . That is,

$$\begin{aligned}
\lambda_1(\mathbf{s}) &= \zeta_1^* \cdot \lambda_{true}(\mathbf{s}); & \log(\zeta_1^*) &\sim N(0, \tau_1^*) \\
\lambda_2(\mathbf{s}) &= \zeta_2^* \cdot \lambda_{true}(\mathbf{s}); & \log(\zeta_2^*) &\sim N(0, \tau_2^*) \\
\lambda_3(\mathbf{s}) &= \zeta_3^* \cdot \lambda_{true}(\mathbf{s}); & \log(\zeta_3^*) &\sim N(0, \tau_3^*) \\
\lambda_4(\mathbf{s}) &= \zeta_4^* \cdot \lambda_{true}(\mathbf{s}); & \log(\zeta_4^*) &\sim N(0, \tau_4^*)
\end{aligned} \tag{3}$$

with  $\zeta_j^* \geq 0$ ,  $j = 1, \dots, 4$  the factors that determine the association between the observed and the true counts for each data source. In order to avoid identifiability issues, we restate the model in (3) in terms of  $\lambda_1(\mathbf{s})$ . That is,

$$\begin{aligned}
\lambda_2(\mathbf{s}) &= \zeta_2 \cdot \lambda_1(\mathbf{s}); & \log(\zeta_2) &\sim N(0, \tau_2) \\
\lambda_3(\mathbf{s}) &= \zeta_3 \cdot \lambda_1(\mathbf{s}); & \log(\zeta_3) &\sim N(0, \tau_3) \\
\lambda_4(\mathbf{s}) &= \zeta_4 \cdot \lambda_1(\mathbf{s}); & \log(\zeta_4) &\sim N(0, \tau_4)
\end{aligned} \tag{4}$$

where  $\zeta_j \geq 0$ ,  $j = \{2, 3, 4\}$ .

### 3.1.2 Model 2

In model 2, we relaxed the assumption of linear relation between the expected value of the number of observations with protocol  $j$ ,  $\lambda_j(\mathbf{s})$ , and the true intensity,  $\lambda_{true}(\mathbf{s})$ , by including terms  $\psi_j^*$ ,  $j = \{1, 2, 3, 4\}$ . That is, we try to explain any deviation from a linear relation between expected values as a function of a GRF  $\omega_1(\mathbf{s})$ . It is worth noting that Model 1 (see above) is a special case of model 2 with  $\psi_j^* = 1$ . We define model 2 as:

$$\begin{aligned}
\lambda_1(\mathbf{s}) &= \zeta_1^* \cdot \lambda_{true}(\mathbf{s}) \cdot \exp\{(\psi_1^* - 1)\omega_1(\mathbf{s})\}; & \log(\zeta_1^*) &\sim N(0, \tau_1^*) \\
\lambda_2(\mathbf{s}) &= \zeta_2^* \cdot \lambda_{true}(\mathbf{s}) \cdot \exp\{(\psi_2^* - 1)\omega_1(\mathbf{s})\}; & \log(\zeta_2^*) &\sim N(0, \tau_2^*) \\
\lambda_3(\mathbf{s}) &= \zeta_3^* \cdot \lambda_{true}(\mathbf{s}) \cdot \exp\{(\psi_3^* - 1)\omega_1(\mathbf{s})\}; & \log(\zeta_3^*) &\sim N(0, \tau_3^*) \\
\lambda_4(\mathbf{s}) &= \zeta_4^* \cdot \lambda_{true}(\mathbf{s}) \cdot \exp\{(\psi_4^* - 1)\omega_1(\mathbf{s})\}; & \log(\zeta_4^*) &\sim N(0, \tau_4^*)
\end{aligned} \tag{5}$$

Again, to avoid identifiability issues, we restate the model in (5) in terms of  $\lambda_1(\mathbf{s})$  as:

$$\begin{aligned}
\lambda_2(\mathbf{s}) &= \zeta_2 \cdot \lambda_1(\mathbf{s}) \cdot \exp\{(\psi_2 - 1) \cdot \omega_1(\mathbf{s})\}; & \log(\zeta_2) &\sim N(0, \tau_2) \\
\lambda_3(\mathbf{s}) &= \zeta_3 \cdot \lambda_1(\mathbf{s}) \cdot \exp\{(\psi_3 - 1) \cdot \omega_1(\mathbf{s})\}; & \log(\zeta_3) &\sim N(0, \tau_3) \\
\lambda_4(\mathbf{s}) &= \zeta_4 \cdot \lambda_1(\mathbf{s}) \cdot \exp\{(\psi_4 - 1) \cdot \omega_1(\mathbf{s})\}; & \log(\zeta_4) &\sim N(0, \tau_4)
\end{aligned} \tag{6}$$

In the scales of the linear predictors in (5),  $\psi_j = \psi_j^* - \psi_1^* + 1$ ,  $j = \{2, 3, 4\}$  are scaling coefficients for the copied GRF,  $\omega_1(\mathbf{s})$ , in each likelihood. Therefore, we would expect posterior densities for  $\psi_3$  and  $\psi_4$  to be around 1. While for  $\psi_2$  we expect different results because line and point counts in Norway do not seem to follow a linear relation (see Section 2; Fig. 2). Due to the different characteristics of line transect surveys in Norway, we propose model 3.

### 3.1.3 Model 3

In addition to causing departure from a linear relation between true and observed counts, species detectability may also change with the census technique used (i.e. one of our data sources, the line transects in TOV-E, targeted only a subset of species as it is regarded as a complementary survey to the point counts). Hence, in model 3 we included a second GRF,  $\omega_2(\mathbf{s})$  to try to account for the characteristics of this observation process. This is included as an additive term in the linear predictor, as follows:

$$\begin{aligned}
\lambda_2(\mathbf{s}) &= \zeta_2 \cdot \lambda_1(\mathbf{s}) \cdot \exp\{(\psi_2 - 1)\omega_1(\mathbf{s})\} \cdot \exp\{\omega_2(\mathbf{s})\} \\
\lambda_3(\mathbf{s}) &= \zeta_3 \cdot \lambda_1(\mathbf{s}) \cdot \exp\{(\psi_3 - 1)\omega_1(\mathbf{s})\} \\
\lambda_4(\mathbf{s}) &= \zeta_4 \cdot \lambda_1(\mathbf{s}) \cdot \exp\{(\psi_4 - 1)\omega_1(\mathbf{s})\}
\end{aligned} \tag{7}$$

We assume a Matérn covariance function as in (2) for  $\omega_2(\mathbf{s})$ , with parameters  $\kappa = \kappa_2$ ,  $\nu = \nu_2$  and  $\sigma^2 = \sigma_2^2$

### 3.1.4 Prior specification

For the GRFs  $\omega_k(\mathbf{s})$ ,  $k = \{1, 2\}$ , the parameters  $\nu_k$  in the Matérn covariance function are fixed to be 1. The interest is put on the spatial ranges  $\rho_k$  and on the standard deviation of the GRFs,  $\sigma_k$ .  $\rho_k$  are related to  $\kappa_k$  through  $\rho_k = \sqrt{8}/\kappa_k$ . The prior distributions of these two parameters are specified by making use of Penalized Complexity (PC) priors, (Fuglstad et al., 2019). In this case, we set  $P(\rho_1 < 20000) = 0.1$  and  $P(\sigma_1 > 1) = 0.1$  for  $\omega_1(\mathbf{s})$ , while  $P(\rho_2 < 2000) = 0.1$  and  $P(\sigma_2 > 3) = 0.1$  for  $\omega_2(\mathbf{s})$ . This means, for example, that under this prior specification, a standard deviation greater than 1 is regarded as large, while a spatial range below 20 kilometers is considered unlikely for  $\omega_1(\mathbf{s})$ . The parameters in  $\beta$  have Normal prior with mean 0 and precision 0.01. Let  $\log(\zeta_j) \sim N(0, \tau_j)$ ,  $j = \{2, 3, 4\}$ , where the logarithm of each  $\tau_j$  has a log-Gamma prior with parameters 1 and 0.00005. For the parameters  $\psi_j$ ,  $j = 2, 3, 4$  in models 2 and 3, we set a normal prior with mean 1 and precision 0.1.

We have now defined a group of three candidate models. In the upcoming subsections, we introduce the methodological approach for fitting them and for selecting a model that suits best for our problem.

## 3.2 Inference and computational approach

The models introduced in Section 3.1 were fitted making use of the Integrated Nested Laplace Approximation (INLA), (Rue et al., 2009) and the SPDE approach (Lindgren et al., 2011). INLA is a faster alternative to Monte Carlo Markov Chains (MCMC) for performing Bayesian inference for latent Gaussian models. INLA aims at producing a numerical approximation of the marginal posterior distribution of the parameters and hyperparameters of the model. Further details can be found in Rue et al. (2009) and Blangiardo and Cameletti (2015). Since we deal with continuous spatial processes in our models, the SPDE approach emerges as an efficient representation of  $\omega_1(\mathbf{s})$  and  $\omega_2(\mathbf{s})$ . It is based on the solution of a SPDE which can be approximated through a basis function representation defined on a triangulation of the spatial domain. More details are available in Lindgren et al. (2011) and Blangiardo and Cameletti (2015).

## 3.3 Model assessment

In order to assess and compare competing models such as the ones we are fitting in upcoming sections, we employed the Deviance Information Criterion (DIC), (Spiegelhalter et al., 2002), the Watanabe-Akaike Information Criterion (WAIC), (Watanabe, 2010), the logarithm of the pseudo marginal likelihood (LPML) ((Blangiardo and Cameletti, 2015)) and the Continuous Rank Probability Score (CRPS) (Gneiting and Raftery, 2007).

DIC makes use of the deviance of the model

$$D(\theta) = -2 \log(p(\mathbf{y}|\theta))$$

to compute the posterior mean deviance  $\bar{D} = E_{\theta|\mathbf{y}}(D(\theta))$ . In order to penalize the complexity of the model, the effective number of parameters,

$$p_D = E_{\theta|\mathbf{y}}(D(\theta)) - D(E_{\theta|\mathbf{y}}(\theta)) = \bar{D} - D(\bar{\theta})$$

is added to  $\bar{D}$ . Thus,

$$DIC = \bar{D} + p_D.$$

The Watanabe-Akaike Information Criterion is based on the posterior predictive density, which makes it preferable to the Akaike and the deviance information criteria, since according to Gelman et al. (2014)



it averages over the posterior distribution rather than conditioning on a point estimate. It is empirically computed as

$$-2 \left[ \sum_{i=1}^n \log \left( \frac{1}{S} \sum_{s=1}^S p(y_i | \theta^s) \right) + \sum_{i=1}^n V_{s=1}^S (\log p(y_i | \theta^s)) \right]$$

with  $\theta^s$  a sample of the posterior distribution and  $V_{s=1}^S$  the sample variance.

Another criterion to compare the models is LMPL, defined as:

$$LMPL = \sum_{i=1}^n \log(CPO_i)$$

It depends on  $CPO_i$ , the Conditional Predictive Ordinate at location  $\mathbf{s}_i$ , (Pettit, 1990), a measure that assesses the model performance by means of leave-one-out cross validation. It is defined as:

$$CPO_i = p(y_i^* | y_f)$$

with  $y_i^*$  the prediction of  $y$  at location  $\mathbf{s}_i$  and  $y_f = y_{-i}$ .

Lastly, we will compare the predictive power of our models using the Continuous Rank Probability Score (CRPS). It makes possible to compare the estimated posterior mean and our observed values while accounting for the uncertainty of the estimation, (Selle et al., 2019). It is defined as:

$$CRPS(F, y) = \int_{-\infty}^{\infty} (F(u) - \mathbf{1}\{y \leq u\})^2 du$$

with  $F$ , the cumulative distribution of the estimated posterior mean, and  $y$  is the observed value. The smaller CRPS is, the closer the estimated value is to the observed one.

## 4 Simulation studies

We set up two simulation studies based on the mid-Scandinavia case that allow us to assess the performance of the models proposed in Section 3, when the true data generating model either assumes linear relation between the counts (Scenario 1) or deviates from this assumption (Scenario 2). We used the same sites as the observations in the TOV-E and BBS surveys (Fig. 1). To start, we simulated the true intensity,  $\lambda_{true}(\mathbf{s})$  as:

$$\log(\lambda_{true}(\mathbf{s})) = \beta_0 + \beta_1 PREC(\mathbf{s}) + \omega_1(\mathbf{s})$$

with  $PREC(\mathbf{s})$ , the precipitation at location  $\mathbf{s}$  in the study region (see Figure S.1.), and  $\omega_1(\mathbf{s})$  a GRF with range  $\rho = 15km$  and  $\sigma^2 = 0.14$ . Further, we specified  $\beta_0 = 4.70$  and  $\beta_1 = -0.20$ . Next, we simulated observations representing the surveys, i.e. using four different Poisson models with parameters  $\lambda_j(\mathbf{s})$ ,  $j = \{1, \dots, 4\}$ . Table 1 summarizes the two simulation scenarios proposed for  $\lambda_j(\mathbf{s})$

Scenario	Simulated $\lambda_j(\mathbf{s})$
1	$\lambda_j(\mathbf{s}) = \zeta_j^* \cdot \lambda_{true}(\mathbf{s})$
2	$\lambda_j(\mathbf{s}) = \zeta_j^* \cdot \lambda_{true}(\mathbf{s}) \cdot \exp((\psi_j^* - 1) \cdot \omega_1(\mathbf{s}))$

Table 1: Simulation scenarios

For each scenario we simulated 100 datasets with  $\zeta_1^* = 0.91$ ,  $\zeta_2^* = 0.04$ ,  $\zeta_3^* = 0.57$  and  $\zeta_4^* = 1.72$ . While we assume a linear relation between  $\lambda_j(\mathbf{s})$  and  $\lambda_{true}(\mathbf{s})$  in Scenario 1, in Scenario 2 the relation between  $\lambda_j(\mathbf{s})$  and  $\lambda_{true}(\mathbf{s})$  is assumed to follow (5) with  $\psi_1^* = 1$ ,  $\psi_2^* = 1.57$ ,  $\psi_3^* = 1.09$  and  $\psi_4^* = 1.21$ . These settings are

based on the posterior distribution of the parameters in the real data case study (presented in Section 5.2). Both simulation scenarios closely mimicked real data application by making two of the simulated counts only observed in Norway, and the other two only observed in Sweden. For each simulated dataset we fitted the three models proposed in Section 3.

To assess the performance of each model in each scenario, we simulated 10000 realizations  $\{\theta_{jkl}^p\}, j = 1, \dots, 10000$ , from the posterior distribution of each parameter  $\theta$  for dataset  $k = 1, \dots, 100$  in scenario  $l = 1, 2$ . Thus, the mean bias and the Root Mean Square Error (RMSE) for dataset  $k$  in scenario  $l$  are computed as:

$$bias_{kl} = \frac{1}{10000} \sum_{j=1}^{10000} (\theta_{jkl}^p - \tilde{\theta})$$

$$RMSE_{kl} = \sqrt{\frac{1}{10000} \sum_{j=1}^{10000} (\theta_{jkl}^p - \tilde{\theta})^2}$$

with  $\tilde{\theta}$  the true value of parameter  $\theta$ .

## 5 Results

### 5.1 Simulation Studies

The 100 datasets generated in each of the two scenarios were fitted using the three proposed models in Section 3 and the results summarized here using the measures of performance introduced in Section 4. We only show the mean bias and RMSE for the parameters  $\zeta_2^*$ ,  $\zeta_3^*$  and  $\zeta_4^*$  as they are key to understand how the different response variables interact with each other (Fig. 3).

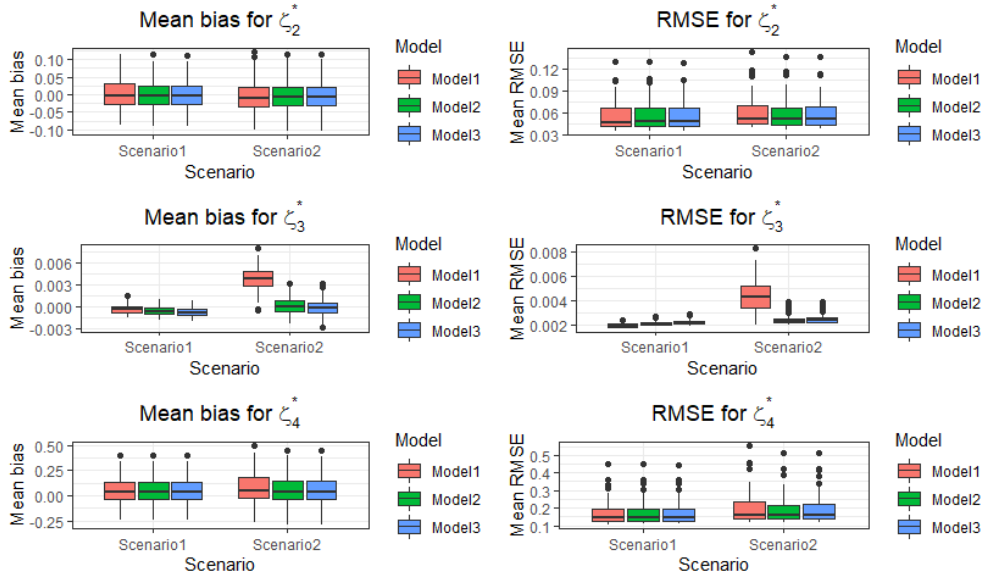


Figure 3: Mean bias (left) and RMSE (right) for parameters  $\zeta_2^*$  (upper panels),  $\zeta_3^*$  (central panels) and  $\zeta_4^*$  (lower panels) for each model in simulation scenarios 1 and 2.

Figure 3 shows that the estimation of the proportional relation between the four likelihoods performed

similarly for the three models when the true is that the four likelihoods are linearly related (Scenario 1). Model 1 performed, as expected, slightly better than the other two models as this is the model that generated the datasets. However, when we introduced some deviation from the assumption of linearity in our data generating process (Scenario 2), Model 1 underperformed relative to the other two models. This is true for the three parameters of interest (Figure 3). While models 2 and 3 perform better in terms of bias and RMSE, the estimates produced by model 1 were biased and showed higher uncertainty.

Scenario	Model	$\beta_0$		$\beta_1$		$\rho$		$\sigma$	
		Bias	RMSE	Bias	RMSE	Bias	RMSE	Bias	RMSE
1	1	-0.110	0.120	$-2.06 \cdot 10^{-4}$	0.041	-499.744	4218.957	0.042	0.064
		(0.037)	(0.034)	(0.028)	(0.011)	(3303.209)	(1719.938)	(0.044)	(0.036)
	2	-0.109	0.119	$-5.44 \cdot 10^{-5}$	0.041	-758.636	4561.989	0.047	0.080
		(0.037)	(0.035)	(0.028)	(0.011)	(3879.115)	(1915.166)	(0.064)	(0.057)
	3	-0.110	0.119	$-6.01 \cdot 10^{-4}$	0.041	-715.139	4714.21	0.046	0.079
		(0.037)	(0.035)	(0.028)	(0.011)	(4037.055)	(1941.135)	(0.065)	(0.055)
2	1	-0.114	0.125	$-7.40 \cdot 10^{-4}$	0.043	136.221	4281.164	0.065	0.082
		(0.036)	(0.034)	(0.028)	(0.011)	(3382.655)	(1929.667)	(0.044)	(0.041)
	2	-0.109	0.120	$-3.42 \cdot 10^{-3}$	0.038	-327.947	4413.111	0.047	0.077
		(0.036)	(0.034)	(0.024)	(0.009)	(3756.358)	(1980.736)	(0.058)	(0.048)
	3	-0.109	0.120	$-3.56 \cdot 10^{-3}$	0.038	-323.678	4508.924	0.050	0.051
		(0.036)	(0.034)	(0.024)	(0.009)	(3882.150)	(2048.977)	(0.061)	(0.077)

Table 2: Mean bias and RMSE for parameters  $\beta_0$ ,  $\beta_1$ ,  $\rho$  and  $\sigma$  in simulation scenarios 1 and 2. In parentheses, the standard error of each performance measurement.

Our results show that there are only marginal differences in the fixed effects  $\beta_0$  and  $\beta_1$  between the three models in both scenarios. However, larger differences are observed for the hyperparameters of  $\omega_1(\mathbf{s})$ . For example, in both scenarios the bias and RMSE of  $\rho$  were smaller for model 1 compared to the other two models. For  $\sigma$ , small differences were observed in Scenario 1, but both bias and RMSE of  $\sigma$  were much smaller for models 2 and 3 than for model 1 in Scenario 2.

## 5.2 Results for TOV-E and BBS data

We fitted our three models (see Section 3) to abundance data from the common bird monitoring programs in Norway and Sweden (see Section 2) with precipitation and elevation as explanatory variables as it was the subset of candidate variables that produced the best results in terms of goodness of fit (see Supplementary Information for an overview of the performance of other competing models). In Table 3, we report the posterior mean, standard deviation and quartiles of the most relevant parameters from the three models.

Table 3 shows the associations between precipitation (PREC) and elevation (ELEV) with the expected counts are negative for all the models. The posterior means of the parameters of these two variables have small differences with stronger association of the explanatory variables and the response variable estimated by model 2. The posterior summaries of PREC and ELEV suggest that those locations with higher levels of precipitation and elevation are expected to have lower counts. The variability and range of the Gaussian field have right skewed posterior distributions based on their posterior medians and means.

Parameter	Model														
	Model 1					Model 2					Model 3				
	Mean	SD	0.025q	0.50q	0.975q	Mean	SD	0.025q	0.50q	0.975q	Mean	SD	0.025q	0.50q	0.975q
Intercept	4.69	0.04	4.61	4.69	4.77	4.68	0.03	4.62	4.68	4.75	4.69	0.04	4.61	4.69	4.77
PREC	-0.12	0.04	-0.19	-0.12	-0.04	-0.20	0.03	-0.26	-0.20	-0.14	-0.11	0.04	-0.18	-0.11	-0.04
ELEV	-0.29	0.04	-0.38	-0.29	-0.21	-0.39	0.04	-0.46	-0.39	-0.32	-0.27	0.04	-0.35	-0.27	-0.19
$\zeta_2$	0.05	0.00	0.04	0.05	0.05	0.04	0.00	0.04	0.04	0.05	0.04	0.00	0.04	0.04	0.05
$\zeta_3$	0.51	0.03	0.45	0.51	0.57	0.48	0.03	0.43	0.48	0.54	0.51	0.03	0.45	0.51	0.57
$\zeta_4$	1.50	0.09	1.33	1.50	1.68	1.42	0.08	1.27	1.42	1.58	1.50	0.09	1.32	1.49	1.69
$\psi_2$						1.86	0.14	1.59	1.86	2.13	1.86	0.16	1.30	1.86	2.13
$\psi_3$						1.26	0.13	1.00	1.26	1.52	1.09	0.12	0.86	1.09	1.34
$\psi_4$						1.30	0.12	1.07	1.30	1.54	1.18	0.12	0.96	1.18	1.42
$\rho$	$1.80 \cdot 10^4$	$4.00 \cdot 10^3$	$1.11 \cdot 10^4$	$1.77 \cdot 10^4$	$2.68 \cdot 10^4$	$1.80 \cdot 10^4$	$3.88 \cdot 10^3$	$1.17 \cdot 10^4$	$1.75 \cdot 10^4$	$2.69 \cdot 10^4$	$2.01 \cdot 10^4$	$4.12 \cdot 10^3$	$1.29 \cdot 10^4$	$1.98 \cdot 10^4$	$2.90 \cdot 10^4$
	0.36	0.02	0.32	0.36	0.41	0.31	0.02	0.27	0.31	0.36	0.34	0.03	0.29	0.34	0.39

Table 3: Posterior mean, standard deviation and quartiles of the most relevant parameters of the models proposed in section 3

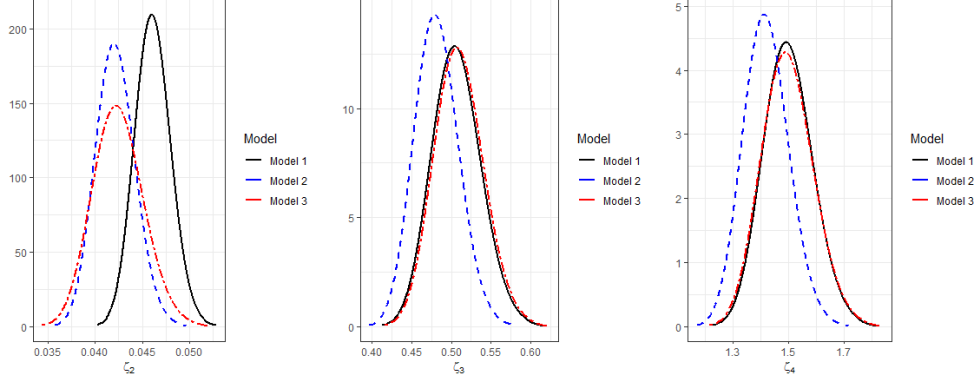


Figure 4: Posterior densities of  $\zeta_2$  (left),  $\zeta_3$  (center) and  $\zeta_4$  (right) for each model

Figure 4 and Table 3 show that the posterior densities of  $\zeta_2$  are different between models, with higher posterior mean compared to the other models. This result agrees with the exploratory analysis of Section 2, which suggested the necessity of specifying a relation between the line and point counts in Norway which relaxed the assumption of linearity. However, the posterior densities of  $\zeta_3$  and  $\zeta_4$  are almost identical for models 1 and 3 whereas the posteriors for the same parameters in model 1 are shifted towards lower values of  $\zeta_3$  and  $\zeta_4$ .

Large differences in the posterior mean of  $\psi_2$  in models 2 and 3 are observed when  $\omega_2(\mathbf{s})$  is introduced to account for the particularities of the sampling protocol of the line counts in Norway. While model 2 gives high prevalence to  $\omega_1(\mathbf{s})$  (posterior mean of  $\psi_2 = 1.90$ ) as determinant of the departure from linear association, model 3 reduces this prevalence (posterior mean of  $\psi_2 = 0.63$ ). We expect these differences in contribution of  $\omega_1(\mathbf{s})$  across models to impact their predictive power. In Figure S.2 we show the posterior mean of  $Y_1(\mathbf{s}) + Y_2(\mathbf{s})$ , understood as a proxy for the total abundance of bird species in our study region. Given the high similarity across the whole region, we focus on a smaller sub-region (red square in Figure 5), which encompasses the locations surrounding Trondheimsfjorden and the Norwegian Sea. Figure 5 also shows the differences in the predicted mean of  $Y_1(\mathbf{s}) + Y_2(\mathbf{s})$  between the three models.

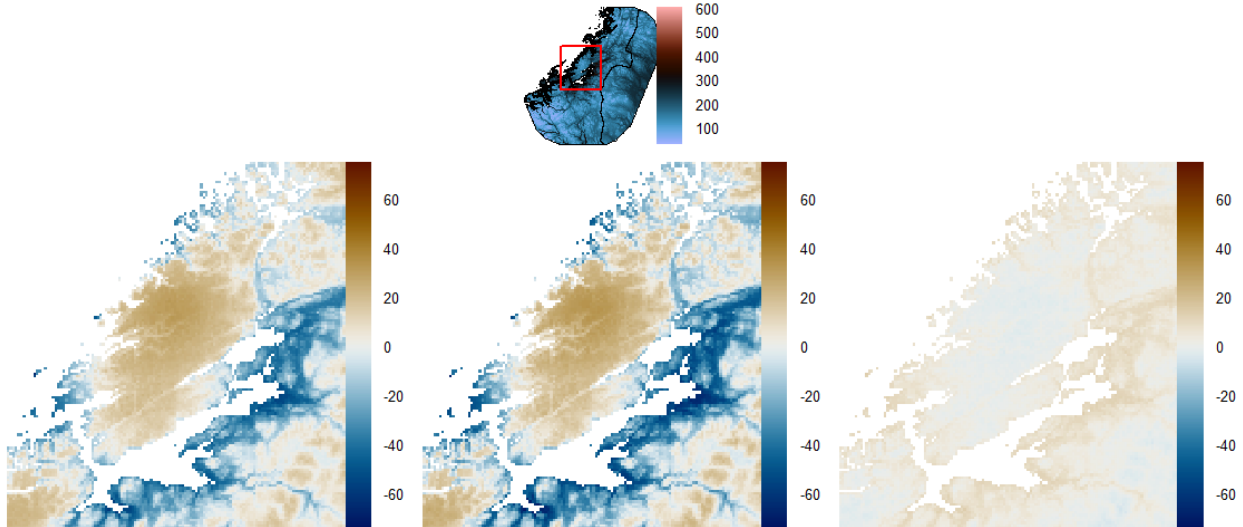


Figure 5: Top (small): Predicted mean of  $Y_1(\mathbf{s}) + Y_2(\mathbf{s})$  using model 2. The red square encloses the zone chosen for analyzing differences between models. Bottom: Differences in the posterior mean of  $Y_1(\mathbf{s}) + Y_2(\mathbf{s})$  between: model 1 and model 2 (model 1 - model 2; left), model 3 and model 2 (model 3 - model 2; center) and model 1 and model 3 (model 1 - model 3; right)

Figure S.3 shows high predicted counts from the three models along the eastern coast of Trondheimsfjorden and on the islands of Hitra and Frøya. Moreover, there are low counts at areas at higher elevations such as those in the southwest and the north of the study region. Figure 5 shows that model 2 produces higher counts compared to the other two models along the fjord’s coast (dark blue) and lower abundance inland (mainly in the mountains; light brown). The differences in predicted counts between model 1 and model 3 are negligible (Figure 5, right panel) compared to those with model 2.

This modeling framework allows us to compute the uncertainty of our predictions. We assess them by computing the standard error of  $Y_1(\mathbf{s}) + Y_2(\mathbf{s})$ . It is displayed for the whole region in Figure S.2, while the differences in standard error for the area highlighted in Figure 5 are shown in Figure 6.

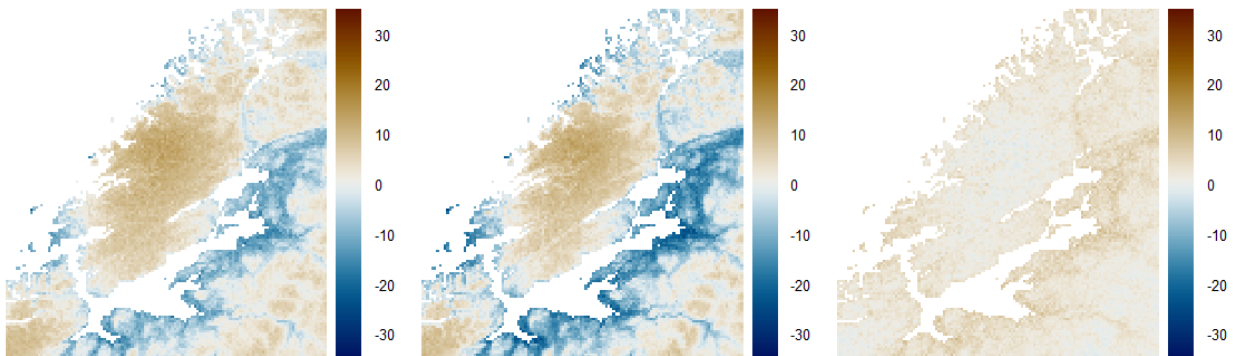


Figure 6: Differences in the posterior standard error of  $Y_1(\mathbf{s}) + Y_2(\mathbf{s})$  for: model 1 and model 2 (model 1 – model 2; left), model 3 and model 2 (model 3 – model 2; center) and model 1 and model 3 (model 1 – model 3; right)

The standard error of model 2 is higher in the coastal areas along the fjord, which is expected because model 2 predicted higher abundances in these areas than the other two models. In most of the areas where models 1 and 3 predicted high counts, larger standard errors are observed, except for a few places where the standard error was similar for the three models. Differences in standard error between models 1 and 3 are negligible in most of the surroundings of the fjord.

To further explore the meaning and importance of a second GRF, in Figure 7 we show the posterior mean of  $\omega_1(\mathbf{s})$  for each model as well as the posterior mean of  $\omega_1(\mathbf{s})$  for model 3. We focus again in the subregion highlighted in Figure 5.

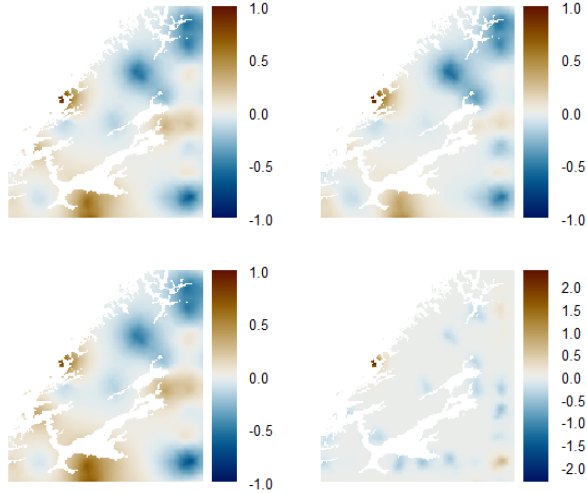


Figure 7: Posterior mean of  $\omega_1(\mathbf{s})$  for models 1 (upper left), 2 (upper right) and 3 (bottom left). Posterior mean of  $\omega_2(\mathbf{s})$  for model 3 (bottom right)

$\omega_1(\mathbf{s})$  is in general similar for the three models. The largest difference occurs in  $\omega_1(\mathbf{s})$  for model 2, which has a shorter range in comparison to the other models. In addition, the highest contribution of  $\omega_2(\mathbf{s})$  occurs in Linesøya, an island where high abundance of birds might be recorded during the line transects, due to high concentrations of geese (mainly greylag goose, *Anser anser*). Such species form large groups of individuals (so called, gaggles) in some of the islands along the Norwegian coast.

Lastly, we compare our three models in terms of goodness of fit and predictive power (Table 4) using the measures of performance introduced in Section 3.3. We only show here the results for the first likelihood (point counts in Norway) of the predictive performance measures as this is the one we use as the reference likelihood in our fitting procedure.

Measure of performance	Model 1	Model 2	Model 3
DIC	2728.79	2751.04	<b>2603.82</b>
WAIC	2876.19	2876.96	<b>2593.69</b>
RMSE	165.60	145.00	<b>38.63</b>
LMPL	-618.41	<b>-616.28</b>	-619.09
Mean CRPS	27.21	25.93	<b>20.95</b>

Table 4: Measures of performance (see Section 3.3) for models 1, 2 and 3. In bold the model with the best performance.

The results show how the goodness of fit is considerably better when we add a second GRF to account for the particular characteristics in one of the observed data sources (line transects in Norway). However, the improvement in predictive power of model 3 in comparison to the other two models is not as evident as for goodness of fit (there is a considerable reduction in RMSE and Mean CRPS, but a smaller value in LMPL). Model 2 does not perform better in terms of goodness of fit, but has better predictive power compared to model 1.

## 6 Discussion and conclusions

The main goal of this paper was to introduce a modeling framework that allows us to model jointly multiple sources of information that are collected following different sampling protocols. More specifically, we focused on bird abundance in Norway and Sweden. These two countries have monitoring programs with

different sampling protocols. Therefore, we proposed a set of models that assumed the same coefficients for the fixed effects in each likelihood and a common GRF. The only difference between the different likelihoods are random intercepts in the linear predictor that aim at accounting for differences in sampling protocols and the units of the counts observed. For example, while the observed point counts in Norway has pairs of birds as the unit reported, Sweden reports individuals. Having different random intercepts makes possible to establish a proportional relation between the observed counts in the data sources. This is arguably a sensible choice since the biological processes that determine the abundance of species do not depend on national borders.

Even though the assumption of linear relation is reasonable for this case, it is also true that when working with real data allowing for some flexibility with respect to this assumption may correspond better to reality. This is why we proposed a model that has a common GRF, but with a coefficient that explains how far we are from a linear relation. As seen in the exploratory analysis (Section 2), one of our data sources did not seem to follow the assumption of linear association with the other likelihoods. Hence, we suggested the inclusion of a second GRF to account for the differences of this likelihood.

We assessed the performance of the three models when the key assumptions in the specification of each of them were not met in a simulation study. Our results showed that a flexible specification did not perform worse than a model that assumed a linear relation when this latter model was used to generate the data. On the other hand, when the linear assumption was not met by the data generating model, the gap in performance between models became more evident. The estimates of the parameters in model 1 (the model assuming a linear relation between the observed counts) were biased and more uncertain than the estimates of the same parameters in the other two models.

The case study of bird abundance in mid-Scandinavia had some atypical counts on the island of Linesøya, found during line sampling, which models 1 and 2 did not explicitly account for. This is arguably why the differences in goodness of fit between models 1 and 2 were not so noticeable. The inclusion of a second GRF to explain particularities of the line counts in Norway (which may produce large number of birds) made sense for our research problem since it was able to explain the large counts in Linesøya, when several species of geese congregate around these islands. Adding GRFs to the likelihoods in order to account for particularities of each observed response seems useful. However, this addition should have a clear justification and be applied with caution since giving an ecological interpretation to this random effect may not be a trivial task.

We want to use the predicted abundance of birds in the region as an input to other models addressing different research questions in applied ecology, such as the risk of death of birds caused by for example powerlines and wind farms (Bernardino et al., 2018; Bevinger, 1995; Bevinger and Broseth, 2001; Serrano et al., 2020). Therefore, the predictive power of our models is of paramount importance to assess the vulnerability of different regions to human development based on the local bird abundance. Although we found differences in goodness of fit between the three models, the differences in predictive power were small. However, a flexible specification for our models seems the best choice for ensuring good predictions. For example, the prediction at the observed locations in Norway were more accurate when using models 2 (which explained a deviation from a linear relation between observed counts using  $\omega_1(\mathbf{s})$ ) and 3 (which also included  $\omega_2(\mathbf{s})$  to account for particularities of the line counts in Norway). This can be understood from the results of the exploratory analysis, which showed that the observed line and point counts in Sweden have a clear linear relation but the Norwegian count data from points and lines did not, as they are only complementary to one another.

In this paper we proposed models to integrate multiple professional surveys with differences in their sampling protocols. These differences are usually determined by the country of origin of the data. The INLA-SPDE approach implemented in the R-INLA package makes it straightforward to integrate multiple sources of information, even if they are not standardized or report the observed counts in different units. A natural extension of this work is the application of the proposed modeling framework to solve a broader range of ecological questions at larger geographical scales that incorporate more sources of information given its



convenience and simple implementation.

## 7 Acknowledgments

The Norwegian terrestrial bird monitoring (TOV-E) is carried out in cooperation between BirdLife Norway and Norwegian Institute for Nature Research, and is financed by the Ministry of Climate and Environment and the Norwegian Environment Agency. The Swedish Bird Survey is supported by grants from the Swedish Environmental Protection Agency, with additional financial and logistic support from the Regional County Boards (Länsstyrelsen).

## Bibliography

- Ahrestani, F. S., Saracco, J. F., Sauer, J. R., Pardieck, K. L., and Royle, J. A. (2017). An integrated population model for bird monitoring in north america. *Ecological Applications*, 27(3):916–924.
- Araújo, M. B., Anderson, R. P., Márcia Barbosa, A., Beale, C. M., Dormann, C. F., Early, R., Garcia, R. A., Guisan, A., Maiorano, L., Naimi, B., O’Hara, R. B., Zimmermann, N. E., and Rahbek, C. (2019). Standards for distribution models in biodiversity assessments. *Science Advances*, 5(1).
- Banerjee, S., Carlin, B. P., and Gelfand, A. E. (2015). *Hierarchical Modeling and Analysis for Spatial Data, Second Edition*. Chapman & Hall/CRC Monographs on Statistics & Applied Probability. CRC Press, 2ed. edition.
- Bernardino, J., Bevanger, K., Barrientos, R., Dwyer, J., Marques, A., Martins, R., Shaw, J., Silva, J., and Moreira, F. (2018). Bird collisions with power lines: State of the art and priority areas for research. *Biological Conservation*, 222:1–13.
- Bevanger, K. (1995). Estimates and population consequences of tetraonid mortality caused by collisions with high tension power lines in norway. *Journal of Applied Ecology*, 32(4):745–753.
- Bevanger, K., Bartzke, G., Brøseth, H., Dahl, E., Gjershaug, J., Hanssen, F., Jacobsen, K.-O., Kleven, O., Kvaløy, P., May, R., Meås, R., Nygård, T., Refsnæs, S., Stokke, S., and Thomassen, J. (2014). Optimal design and routing of power lines: ecological, technical and economic perspectives (optipol). final report: findings 2009-2014.
- Bevanger, K. and Broseth, H. (2001). Bird collisions with power lines - an experiment with ptarmigan (*lagopus* spp.). *Biological Conservation*, 99(3):341–346.
- Blangiardo, M. and Cameletti, M. (2015). *Spatial and spatio-temporal Bayesian models with R-INLA*. John Wiley & Sons.
- Brodie, S. J., Thorson, J. T., Carroll, G., Hazen, E. L., Bograd, S., Haltuch, M. A., Holsman, K. K., Kotwicki, S., Samhouri, J. F., Willis-Norton, E., and Selden, R. L. (2020). Trade-offs in covariate selection for species distribution models: a methodological comparison. *Ecography*, 43(1):11–24.
- Cameletti, M., Gómez-Rubio, V., and Blangiardo, M. (2019). Bayesian modelling for spatially misaligned health and air pollution data through the INLA-SPDE approach. *Spatial Statistics*, 31:100353.
- Fuglstad, G.-A., Simpson, D., Lindgren, F., and Rue, H. (2019). Constructing Priors that Penalize the Complexity of Gaussian Random Fields. *Journal of the American Statistical Association*, 114(525):445–452.
- Gelman, A., Hwang, J., and Vehtari, A. (2014). Understanding predictive information criteria for Bayesian models. *Statistics and Computing*, 24(6):997–1016.
- Gneiting, T. and Raftery, A. E. (2007). Strictly proper scoring rules, prediction, and estimation. *Journal of the American Statistical Association*, 102(477):359–378.

- Gruss, A. and Thorson, J. T. (2019). Developing spatio-temporal models using multiple data types for evaluating population trends and habitat usage. *ICES Journal of Marine Science*, 76(6):1748–1761.
- Howard, C., Stephens, P. A., Pearce-Higgins, J. W., Gregory, R. D., and Willis, S. G. (2014). Improving species distribution models: the value of data on abundance. *Methods in Ecology and Evolution*, 5(6):506–513.
- Johnston, A., Fink, D., Reynolds, M. D., Hochachka, W. M., Sullivan, B. L., Bruns, N. E., Hallstein, E., Merrifield, M. S., Matsumoto, S., and Kelling, S. (2015). Abundance models improve spatial and temporal prioritization of conservation resources. *Ecological Applications*, 25(7):1749–1756.
- Kéry, M. and Royle, J. A. (2009). *Inference About Species Richness and Community Structure Using Species-Specific Occupancy Models in the National Swiss Breeding Bird Survey MHB*, pages 639–656. Springer US, Boston, MA.
- Krainski, E. T. (2019). *Advanced spatial modeling with stochastic partial differential equations using R and INLA*. CRC Press.
- Kålås, J. (2010). The 2010 norwegian red list for species.
- Kålås, J. and Husby, M. (2002). Ekstensiv overvaking av terrestre fugl i norge.
- Lehikoinen, A., Brotons, L., Calladine, J., C. T., Escandell, V., Flousek, J., Grueneberg, C., Haas, F., Harris, S., Herrando, S., H. M., Jiguet, F., Kålås, J. A., Lindström, A., Lorrilliere, R., Molina, B., Pladevall, C., Calvi, G., Sattler, T., Schmid, H., and Trautmann, S. (2019). Declining population trends of european mountain birds. *Global change biology*, 25(2):577–588.
- Lehikoinen, A., Green, M., Husby, M., Kålås, J. A., and Lindström, A. (2014). Common montane birds are declining in northern europe. *Journal of Avian Biology*, 45(1):3–14.
- Lindgren, F., Rue, H., and Lindström, J. (2011). An explicit link between Gaussian fields and Gaussian Markov random fields: the stochastic partial differential equation approach. *Journal of the Royal Statistical Society: Series B (Statistical Methodology)*, 73(4):423–498.
- Lindstrom, A., Green, M., Paulson, G., Smith, H. G., and Devictor, V. (2013). Rapid changes in bird community composition at multiple temporal and spatial scales in response to recent climate change. *Ecography*, 36(3):313–322.
- May, R., Middel, H., Stokke, B. G., Jackson, C., and Verones, F. (2020). Global life-cycle impacts of onshore wind-power plants on bird richness. *Environmental and Sustainability Indicators*, 8:100080.
- Oedekoven, C. S., Elston, D. A., Harrison, P. J., Brewer, M. J., Buckland, S. T., Johnston, A., Foster, S., and Pearce-Higgins, J. W. (2017). Attributing changes in the distribution of species abundance to weather variables using the example of british breeding birds. *Methods in Ecology and Evolution*, 8(12):1690–1702.
- Pettit, L. I. (1990). The Conditional Predictive Ordinate for the Normal Distribution. *Journal of the Royal Statistical Society: Series B (Methodological)*, 52(1):175–184.
- Roksvåg, T., Steinsland, I., and Engeland, K. (2020). A geostatistical two field model that combines point observations and nested areal observations, and quantifies long-term spatial variability – a case study of annual runoff predictions in the voss area.
- Rue, H. and Held, L. (2005). *Gaussian Markov random fields: theory and applications*. Monographs on statistics and applied probability 104. Chapman & Hall CRC, 1 edition.
- Rue, H., Martino, S., and Chopin, N. (2009). Approximate Bayesian inference for latent Gaussian models by using integrated nested Laplace approximations. *Journal of the Royal Statistical Society: Series B (Statistical Methodology)*, 71(2):319–392.

- Selle, M. L., Steinsland, I., Hickey, J. M., and Gorjanc, G. (2019). Flexible modelling of spatial variation in agricultural field trials with the r package *inla*. *Theoretical and Applied Genetics*, 132(12):3277–3293.
- Serrano, D., Margalida, A., Pérez-García, J. M., Juste, J., Traba, J., Valera, F., Carrete, M., Aihartza, J., Real, J., Mañosa, S., Flaquer, C., Garin, I., Morales, M. B., Alcalde, J. T., Arroyo, B., Sánchez-Zapata, J. A., Blanco, G., Negro, J. J., Tella, J. L., Ibañez, C., Tellería, J. L., Hiraldo, F., and Donazar, J. A. (2020). Renewables in Spain threaten biodiversity. *Science*, 370(6522):1282–1283.
- Simpson, D., Illian, J. B., Lindgren, F., Sørbye, S. H., and Rue, H. (2016). Going off grid: computationally efficient inference for log-Gaussian Cox processes. *Biometrika*, 103(1):49–70.
- Soykan, C. U., Sauer, J., Schuetz, J. G., LeBaron, G. S., Dale, K., and Langham, G. M. (2016). Population trends for north American winter birds based on hierarchical models. *Ecosphere*, 7(5):e01351.
- Spiegelhalter, D. J., Best, N. G., Carlin, B. P., and Van Der Linde, A. (2002). Bayesian measures of model complexity and fit. *Journal of the Royal Statistical Society: Series B (Statistical Methodology)*, 64(4):583–639.
- Stroud, D. A., Madsen, J., and Fox, A. D. (2017). Key actions towards the sustainable management of European geese. *Ambio*, 46(2):328–338.
- Watanabe, S. (2010). Asymptotic Equivalence of Bayes Cross Validation and Widely Applicable Information Criterion in Singular Learning Theory. *J. Mach. Learn. Res.*, 11:3571–3594.
- Yu, H., Cooper, A. R., and Infante, D. M. (2020). Improving species distribution model predictive accuracy using species abundance: Application with boosted regression trees. *Ecological Modelling*, 432:109202.